Double-modulation stimulated Raman scattering: how to image up to 16-fold faster

Sandro Heuke, Xavier Audier, Hervé Rigneault

Double-modulation stimulated Raman scattering (DM-SRS): how to image up to 16-fold faster

SANDRO HEUKE[1,*], XAVIER AUDIER[2], AND HERVÉ RIGNEAULT[1,*]

[1] Aix Marseille Univ, CNRS, Centrale Marseille, Institut Fresnel, Marseille, France.
[2] Department of Chemistry & Biochemistry, Georgia Institute of Technology, Atlanta, USA.
[*] Corresponding authors: sandro.heuke@fresnel.fr & herve.rigneault@fresnel.fr

Compiled January 22, 2024

Stimulated Raman microscope is conventionally performed by modulating either the pump or Stokes beam and demodulating the other. Here, we propose a double modulation scheme that modulates both beams at f_m and $2f_m$. Exploiting aliasing and reduction of the repetition rate, we show that the proposed double modulation scheme amplifies the signal amplitude by a factor of 1.5, 2 and 4 for different modulation frequencies and experimental realizations for the same average power at the sample. By deriving the noise power for different sources, we show that the double modulation scheme can perform SRS imaging with an up to 16-fold speed improvement as compared to single beam modulation.

http://dx.doi.org/10.1364/ao.XX.XXXXXX

Laser scanning stimulated Raman scattering (SRS) is a nonlinear microscopy technique targeting specific molecular vibrations [1–3]. Among the numerous applications discovered, the preresonant SRS imaging of alkine [4], and C-D labeled dyes [5] as well as stimulated Raman histopatholgy (SRH) [6, 7] hold the greatest potential to leave optical labs and enter hospitals or biolabs with game-changing consequences, e.g. for diagnosing and staging of various diseases. Imaging of low concentrated dyes demands for the highest sensitivity whereas SRH requires high sample throughputs at best image acquisition rates. For a given pulse width and spectral resolution, the sensitivity and imaging speed of SRS is fundamentally limited by the damage threshold of the sample and the noise characteristics of the laser source.

At best, the latter is shot-noise limited and possesses the smallest possible repetition rate due to its inverse quadratic relation to the signal-to-noise (SNR) for a constant average power. Today, state-of-the-art light sources used for SRS imaging can be grouped into: high-noise fiber laser with customized repetition rates [8–10] and shot-noise limited solid-state lasers working around 80 MHz [1, 3]. To the best of our knowledge, only one shot-noise limited fiber laser was reported in the context SRS imaging [11]. As a second strategy to reduce the impact of excess noise, balanced detection allows to approach the shot-noise limit up to a distance of 3dB [9]. Nevertheless, auto-balanced photo-diodes [8] for the range of 800-1100 nm and high reverse voltages bias are not yet commercially available.

As the major competitor of fiber laser, shot-noise limited solid-state laser with nearly transform limited pulses are commercially available within a wide spectral and temporal pulse-width range. As the limiting factor, their repetition rate is frequently fixed around 80 MHz. Its rep rate reduction would require an inverse proportional extension of the laser cavity leading to, e.g. a 8 m sized ring resonator cavity to obtain a 40 MHz oscillator, with increasing noise problems arising from mechanical instabilities and air convection within the cavity. From a practical point of view, best sensitivities in SRS-imaging can be expected, therefore, either from a shot-noise

	Standard SRS		DM-SRS		Pulse-Picked SRS
f_m	$< f_r/2$	$= f_r/2$	$< f_r/4$	$= f_r/4$	$f_m = f_r/4$
$M_{st}(t)$	$1+\cos(2\pi f_m t)$		$1+\cos(2\pi f_m t)$		$(1+\cos(2\pi f_m t))(1+\cos(4\pi f_m t))$
$M_{pu}(t)$	1		$1+\cos(4\pi f_m t)$		$1+\cos(4\pi f_m t)$
P_{SRS} / P_{Excess} / P_{Shot}	1/1/1	$2^2/2^2/2$	$1.5^2/1.5^2/1.5$	$2^2/2^2/2$	$4^2/2^2/2$
SNR_{ex} / SNR_{shot} / SNR_{el}	1/1/1	1/2/4	1/1.5/2.25	1/2/4	4/8/16

Table 1. Overview about the modulations schemes and theoretical power alterations of the SRS signal, noise contributions and resulting $SNR = P_{SRS}/P_{noise}$ considering a dominant noise source (laser excess, shot- or electrical noise).

limited solid state laser at 80 MHz that will be outperformed only by perfectly auto-balanced fiber laser featuring the same pulse characteristics and repetition rates $f_r \leq 40$ MHz to compensate for the sensitivity loss of the balanced detection. If position-multiplexing, such as dual- or multi-focus approaches [12], is already installed or not useful to be implemented only few options for a significant SNR improvement remain. The perhaps most intriguing approach was highlighted by Ozeki et al. by exploiting an aliasing effect while modulating the laser at exactly half the laser's repetition rate (38 MHz) to gain a factor 2 in shot-noise limited SNR [13]. For solid-state laser systems the detection and demodulation at half the laser's repetition rate is electronically demanding and favors photodiodes with unpractical small photo-active areas. Here, we present a second route to exploit an aliasing effect by modulating both the pump and the Stokes laser at $f_1=f_m$ and $f_2=2f_m$. By introducing a modulation of one laser at twice the lock-in frequency (≤ 20 MHz) we can benefit from a sub-harmonic enhancement similar to what Ozeki and coworkers reported [13]. Furthermore, if the pump beam is modulated at both $f_1=f_r/4$ and $f_2=f_r/2$, the beam is effectively pulse-picked and an SNR improvement of a factor of up to 16 can be expected if the average power at the sample is kept constant.

For the derivation of the aliasing effect we follow the notation introduced in a previous noise tutorial [14]. The photo-diode returns the voltage of the SRS-signal at a strength of:

$$U_{SRS} = \Big[\sum_{k=-\infty}^{+\infty} X_k h(t-t_k) + \epsilon(t) \Big] \times g\sqrt{2}R\cos(2\pi f_m t) \tag{1}$$

Where the term in large brackets is $I_{SRS}(t)$, the photocurrent output of the detector. $G(t) = g\sqrt{2}R\cos(2\pi f_m t)$ represents the lock-in amplification with load R and gain g. $\epsilon(t)$ is the electronic noise in the detection, modeled by a random noise of zero average mean and power spectral density $S_\epsilon(f)$. $h(t)$ is the response function of the detector to a single photon arrival, which can be approximated by $q\delta(t)$ for all practical purposes with q being the electric charge of a single photo-electron. X_k denotes the random variable that describes the number of photons detected on the probe pulse arriving at $t_k = k/f_r$. The statistics of X_k is related to: (1) The time-average number of photons on the pump and Stokes lasers, N_{pu} and N_{st}. They are kept constant across all measurement schemes to compare SNR levels at a fixed average optical power. (2) The time modulation applied on the pump and Stokes lasers, $M_{pu}(t)$ and $M_{st}(t)$. (3) The modulation transfer β due to the SRS process. (4) The excess laser noise, in the form of a random variable α of unit mean and power spectral density $S_\alpha(f)$. The (ensemble) average value and variance of X_k can be described as:

$$\langle X_k \rangle = N(t_k) = N_{pu} M_{pu}(t_k)[1 + \beta N_{st} M_{st}(t_k)] \tag{2}$$

$$\langle X_k X_l \rangle = N(t_k)N(t_l)\langle \alpha(t_k)\alpha(t_l)\rangle + \delta_{k,l} N(t_k) \tag{3}$$

With these definitions we can calculate the signal power P_{DC}, associated with the DC power of the lock-in output, and the noise power P_N, associated with the power spectral density of the lock-in output within its bandwidth where $f \approx 0$.

$$P_N = \frac{1}{R} S_U(f) = \frac{1}{R} \lim_{T\to+\infty} \frac{1}{T} \langle \left| \hat{U}_T(f) \right|^2 \rangle \tag{4}$$

$$P_{DC} = P_{SRS} = \frac{1}{R} \lim_{T\to+\infty} \left| \frac{1}{T} \langle \hat{U}_T(0) \rangle \right|^2 \tag{5}$$

with the finite-time Fourier transform $\mathcal{F}[U]_T(f) = \hat{U}_T(f) = \int_{t=-T/2}^{T/2} U_{SRS}(t) e^{2i\pi ft} \mathrm{d}t$. Equation 1 can be injected into Eqs 4 and 5, then computed using 2 and 3. The following simplifications make the computation easier: the impact of the second laser is neglected for the noise calculation P_N. The ensemble average values of ϵ and α are zero and one. We call δ the Dirac distribution, and $\mathrm{III}_{T_r} = \sum_{k=-\infty}^{+\infty} \delta(t - kT_r)$ the Dirac train of period T_r. We simplify and express them using the convolution operator $\otimes$. The noise power is separated into three components :

$$P_{SRS} = \frac{q\beta N_{pu} N_{st}}{R} \lim_{T\to+\infty} \frac{1}{T} \left| \mathcal{F}_T[\mathrm{III}_{T_r} M_{st} M_{pu} G](0) \right|^2 \tag{6}$$

$$P_N = P_{Excess} + P_{Shot} + P_{Elec} \tag{7}$$

$$P_{Excess} = \frac{q^2 N_{pu}^2}{R} \lim_{T\to+\infty} \frac{1}{T} \langle \left| \mathcal{F}_T[\mathrm{III}_{T_r} M_{pu} \alpha G](f) \right|^2 \rangle \tag{8}$$

$$P_{Shot} = \frac{q^2 N_{pu}}{R} \lim_{T\to+\infty} \frac{1}{T} \mathcal{F}_T[\mathrm{III}_{T_r} M_{pu} G^2](f) \tag{9}$$

$$P_{Elec} = \frac{1}{R} \lim_{T\to+\infty} \frac{1}{T} \langle \left| \mathcal{F}_T[\epsilon G](f) \right|^2 \rangle \tag{10}$$

While those expressions are simplified they still require computation for the different modulation schemes. The only assumptions are that the laser excess noise $S_\alpha(f)$ decreases quickly with f and has no expected correlations between frequencies. Briefly, the product in time domain, or equivalently the convolution in spectral domain, between the different functions will generate an aliasing effect effectively increasing the signal and noise values. We decide to illustrate the computation in the case of shot-noise power for the DM-SRS case, as it shows in a concise way the ideal use case for this implementation:

$$P_{Shot} = \frac{q^2 N_{pu}}{R} \lim_{T\to+\infty} A_T(f) \tag{11}$$

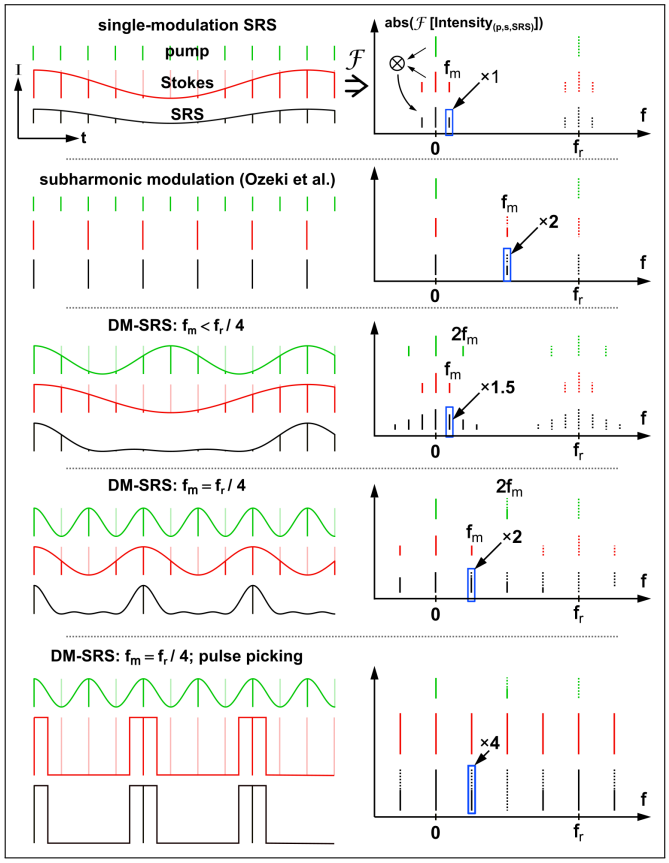

Fig. 1. Double modulation(DM-) SRS scheme: the left and right column show the pump and Stokes beam intensity over time and in Fourier-space, respectively, for different modulation configurations. The pump and Stokes are marked in green and red, respectively. Outlined in black, the SRS-signal is measured as Stimulated Raman Loss (SRL) with $I_{SRS} \propto I_p I_S$ and $\mathcal{F}[I_{SRS}] \propto \mathcal{F}[I_p] \otimes \mathcal{F}[I_S]$. f_r and f_m are the laser repetition rate and modulation frequency, respectively.

with

$$A_T(f) = \frac{1}{T}\Big[\mathcal{F}_T[\text{Ш}_{T_r}] \otimes \hat{M}_{pu} \otimes \hat{G} \otimes \hat{G}\Big](f) \tag{12}$$

$$= \frac{2g^2R^2}{T}\Big[\sum_{k|kT_r\in[0,T]} e^{i2\pi k\frac{f}{f_r}} \otimes \Big(\delta(f) + \frac{1}{2}\delta(f \pm 2f_m)\Big)$$

$$\otimes \frac{1}{2}\delta(f \pm f_m) \otimes \frac{1}{2}\delta(f \pm f_m)\Big](f) \tag{13}$$

$$\underset{f\to 0}{=} \frac{2g^2R^2}{T} \sum_{k|kT_r\in[0,T]} \frac{1}{8}\Big[6 + 4e^{\pm i2\pi k\frac{2f_m}{f_r}} + e^{\pm i2\pi k\frac{4f_m}{f_r}}\Big] \tag{14}$$

We care about the noise at $f \approx 0$ as this will be the frequency band where our signal is detected at the output of the lock-in. The exponential terms in bracket in Eq. 14 will average out to 0 when $T \to \infty$ unless $f_m = f_r/2$ or $f_r/4$. The first case is equivalent to standard single modulation (SM)-SRS with half repetition rate modulation. The case $f_m = f_r/4$ give a total sum of 1 as opposed to 3/4 for all other cases. Since the conventional SRS implementation (SM-SRS, $f_m < f_r/2$) without modulation gives a factor of 1/2, the increase in shot-noise power is 3/2 and 2 for $f_m < f_r/4$ and $f_m = f_r/4$, respectively.

The modulation of the pump and Stokes beams for the schemes discussed in this paper, as well as the computed signal and noise powers, are summarized in Table 1. We observe that the power of the SRS signal increase by 2.25 up to 16-fold in dependence of the type of modulation scheme. A more visual explanation for the signal improvement in DM-SRS is provided in Figure 1. In time domain, our modulation schemes try to increase the maximum SRS signal amplitude. The maximum SRS amplitude transfer will arise when both pump and Stokes pulses achieve their maximum peak power. Any set of pulse where the pump or Stokes beams are at an intermediate power level do not contribute as much to the SRS signal, which is measured as the difference between the maximum on and off state. Thus, the pulse energy of intermediate pulses is exploited better if added to those pulses in full "on" state. As a result, one can suppress the pump beam during the time it takes for the Stokes beam to go from it's minimum to maximum value. In the frequency domain one can interpret the results as the aliasing of high frequencies which add to the overall signal strength - see the right column of Fig. 1. Nevertheless, the additional modulation in DM-SRS also introduces noise in dependence of the modulation

scheme, even if the modulation itself is perfectly clean. Since the electric noise P_{Elec} does not depend on the modulation scheme, the best improvement in SNR will appear for systems that are limited by their electronic noise. While it would always be beneficial to reduce the electronic noise, the constraints on a SRS system can be such that the measurement is limited by its electronics, e.g. for Epi-SRS featuring weak optical power levels at the detector.

On the contrary, for a SRS system limited by its laser excess noise, the modulation scheme applied to the pump beam will not improve the measurement SNR [15], and a balanced detection or an additional modulation of the Stokes beam will be necessary to further improve the system's SNR. As a less intuitive result, DM-SRS also enhances the shot-noise though the average power and, therefore, the overall number of photons detected is kept constant. This phenomenon can be understood from the impact of the lock-in amplification G(t). In SM-SRS, the SRS signal is multiplied by a cosine at values between -1 and 1. The average absolute value of the modulation is, therefore, 0.5. When laser pulses arrive at the detector in DM-SRS, however, this amplifications is always either 1 or -1 yielding a gain of absolute value 1. Thus, DM-SRS is not only amplifying better the SRS signal but also the shot-noise on top of the laser.

As a limitation of our model, we assume that the Stokes laser (not detected) has no noise. In most case, the noise of the modulated laser is not considered to have dominant impact, since the modulation transfer β is on the order of 10^{-4}-10^{-6}. For high SNR measurements, however, we can expect that this laser will introduce additional noise that can overpower the noise-level of the detected laser. Second , we assume that the modulation imprinted on both lasers has pure frequency components. While some devices like resonant EOMs may not affect the noise below their resonant frequency, acousto-optic modulators (AOM) can introduces considerable amounts of noise reducing the SNR.

In the following, DM-SRS' predicted signal improvements are demonstrated experimentally for the cases $f_m = f_r/4$ with and without pulse picking (i.e. double modulation of a single beam). Figure 2 displays our experimental implementation and modulation scheme. The basic setup was described elsewhere [16]. Briefly, an 80 MHz Yb-fiber laser (APE Emerald engine) is used to pump two optical parametric oscillators (OPO, APE Emerald). OPO1 provides the pump beam and is modulated at $f_1 = f_r/2 = 40$ MHz using a resonant EOM (APE, EOM 900) for DM-SRS. For the pulse-picked DM-SRS, the EOM was placed closer to the microscope to allow for modulation of both beams at 40 MHz. The Stokes beam is generated by OPO2 and modulated by an AOM (AA, MT200-B100A0,5-800) at $f_2 = f_r/4 = 20$ MHz. If the Stokes beam is modulated in addition by the EOM a pulsing-picking scenario is created cropping one out of 4 pulses. The light is focused via a 40$\times$ objective onto the sample, collected by a condenser lens and detected by a photo-diode (PD, APE SRS photodiode). The latter is coupled to a electrical band pass-filter (Mini-Circuits, BBP-21.4+), to remove the 40 MHz modulation, and connected to a lock-in amplifier (Zurich Instruments, HF2LI) that demodulates the SRS signal at 20 MHz. The pump and Stokes beam were tuned to 2930 cm^{-1} and focused into olive oil with an average power below 20 mW for both colors combined. Figure 2 a displays the SRS-signal over 3 s for DM- and SM-SRS for a dwell time of 40 µs. The average power entering the microscope was kept constant for both modulation schemes and colors. Comparing DM- and SM-SRS, it is observed that the signal amplitude is increased by a factor of 1.9 while the average SNR was increased by a factor of 3.4. The SNR improvement close to 4 indicates that the measurement is limited by electrical noise for this particular input power. The difference to the theoretical values of 2 for the signal and 4 for the SNR can be explained by an insufficient modulation of the EOM which may not have achieved a 100 % suppression of every second pulse. To demonstrate the benefit of DM-SRS in application to histopathology samples, we imaged a 10 µm thick human colon section. The corresponding raw images are presented in Fig. 2 c and 2 e. In contrast to SM-SRS, the improved image quality of DM-SRS allows to distinguish colon crypts as well as the profile of nuclei which is a fundamental requirement for stimulated Raman histopathology applications. For the pulse-picked DM-SRS, we measured as well the signal and noise levels for an oil-sample as highlighted in Fig. 2 b. It is found that the signal level increased by a factor of 3.8 while the SNR gained a factor of 15, which is in reasonable agreement with the expected improvement of 4 and 16. To highlight the impact of such an enhancement of SNR, we imaged a human breast tissue section of 20 µm thickness at the Raman resonance of 2930 cm^{-1} as shown in Fig. 2 d and f. While the lipid droplets are clearly visible for both the pulse-picked DM- and SM-SRS images, the structure of the surrounding connective tissue is hardly perceptible in SM-SRS. Thus, pulse-picked DM-SRS significantly increases the image SNR and quality allowing to extract morphological details which would be unrecognizable otherwise. Clearly, this SNR enhancement is readily translated into an improvement of the detection limit of a certain Raman-active molecular group or empowers the user to accelerate the image acquisition.

FUNDING INFORMATION

INSERM (18CP128-00, PC201508); Agence Nationale de la Recherche (ANR-10-INSB-04-01, ANR-11-INSB-0006, ANR-16-CONV-0001, ANR-19-CE19-0019-02, ANR-11-IDEX-0001-02, ANR-21-ESRE-0002 IDEC); Région Sud; Institut National Du Cancer; Cancéropôle Provence-Alpes-Côte d'Azur; Centre National de la Recherche Scientifique; EU ICT 101016923 CRIMSON

DISCLOSURE

The authors declare no conflict of interest.

REFERENCES

1. C. W. Freudiger, W. Min, B. G. Saar, S. Lu, G. R. Holtom, C. He, J. C. Tsai, J. X. Kang, and X. S. Xie, Science **322**, 1857 (2008).
2. P. Nandakumar, A. Kovalev, and A. Volkmer, New J. Phys. **11**, 033026 (2009).
3. Y. Ozeki, F. Dake, S. Kajiyama, K. Fukui, and K. Itoh, Opt. Express **17**, 3651 (2009).
4. L. Wei, F. Hu, Y. Shen, Z. Chen, Y. Yu, C.-C. Lin, M. C. Wang, and W. Min, Nat. Methods **11**, 410 (2014).
5. L. Shi, C. Zheng, Y. Shen, Z. Chen, E. S. Silveira, L. Zhang, M. Wei, C. Liu, C. de Sena-Tomas, K. Targoff, and W. Min, Nat. Commun. **9** (2018).

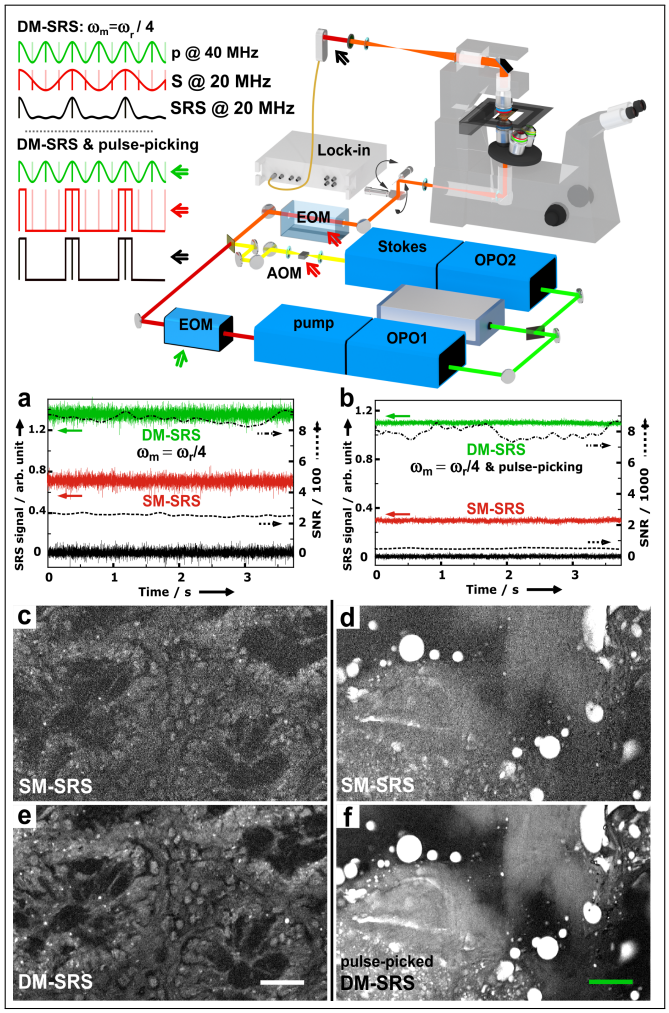

Fig. 2. Experimental setup and results: The position of the EOM is moved from the OPO1 beam path for DM-SRS into the combined beam path to enable pulse-picked DM-SRS. a) and b) the green and the red lines represent DM-SRS (or pulse picked DM-SRS) and SM-SRS signal, respectively. The photo-diode's dark current is outlined in black. The dash-dotted and dashed black curves are the SNR of DM- and SM-SRS, respectively. e) and f) show the DM-SRS and pulse picked DM-SRS images of a human colon tissue and human breast tissue section, respectively. c) and d) display the corresponding images using SM-SRS for the same average power. Scale bars 20 µm. Pixel dwell time 40 µs.

6. D. A. Orringer, B. Pandian, Y. S. Niknafs, T. C. Hollon, J. Boyle, S. Lewis, M. Garrard, S. L. Hervey-Jumper, H. J. L. Garton, C. O. Maher, J. A. Heth, O. Sagher, D. A. Wilkinson, M. Snuderl, S. Venneti, S. H. Ramkissoon, K. A. McFadden, A. Fisher-Hubbard, A. P. Lieberman, T. D. Johnson, X. S. Xie, J. K. Trautman, C. W. Freudiger, and S. Camelo-Piragua, Nat. Biomed. Eng. **1**, 0027 (2017).
7. B. Sarri, R. Canonge, X. Audier, E. Simon, J. Wojak, F. Caillol, C. Cador, D. Marguet, F. Poizat, M. Giovannini, and H. Rigneault, Sci. Reports **9** (2019).
8. C. W. Freudiger, W. Yang, G. R. Holtom, N. Peyghambarian, X. S. Xie, and K. Q. Kieu, Nat. Photonics **8**, 153 (2014).
9. K. Nose, Y. Ozeki, T. Kishi, K. Sumimura, N. Nishizawa, K. Fukui, Y. Kanematsu, and K. Itoh, Opt. Express **20**, 13958 (2012).
10. S. Heuke, B. Sarri, X. Audier, and H. Rigneault, Opt. Lett. **43**, 3582 (2018).
11. G. Dai, K. Katoh, and Y. Ozeki, Opt. Express **29**, 11702 (2021).
12. S. Heuke, B. Sarri, A. Lombardini, X. Audier, and H. Rigneault, Opt. Lett. **43**, 4763 (2018).
13. Y. Ozeki, Y. Kitagawa, K. Sumimura, N. Nishizawa, W. Umemura, S. Kajiyama, K. Fukui, and K. Itoh, Opt. Express **18**, 13708 (2010).
14. X. Audier, S. Heuke, P. Volz, I. Rimke, and H. Rigneault, APL Photonics **5**, 011101 (2020).
15. C. Gohle, J. Rauschenberger, T. Fuji, T. Udem, A. Apolonski, F. Krausz, and T. W. Hänsch, Opt. Lett. **30**, 2487 (2005).
16. S. Brustlein, P. Ferrand, N. Walther, S. Brasselet, C. Billaudeau, D. Marguet, and H. Rigneault, J. Biomed. Opt. **16**, 021106 (2011).

REFERENCES

1. C. W. Freudiger, W. Min, B. G. Saar, S. Lu, G. R. Holtom, C. He, J. C. Tsai, J. X. Kang, and X. S. Xie, Science **322**, 1857 (2008).
2. P. Nandakumar, A. Kovalev, and A. Volkmer, New J. Phys. **11**, 033026 (2009).
3. Y. Ozeki, F. Dake, S. Kajiyama, K. Fukui, and K. Itoh, Opt. Express **17**, 3651 (2009).
4. L. Wei, F. Hu, Y. Shen, Z. Chen, Y. Yu, C.-C. Lin, M. C. Wang, and W. Min, Nat. Methods **11**, 410 (2014).
5. L. Shi, C. Zheng, Y. Shen, Z. Chen, E. S. Silveira, L. Zhang, M. Wei, C. Liu, C. de Sena-Tomas, K. Targoff, and W. Min, Nat. Commun. **9** (2018).
6. D. A. Orringer, B. Pandian, Y. S. Niknafs, T. C. Hollon, J. Boyle, S. Lewis, M. Garrard, S. L. Hervey-Jumper, H. J. L. Garton, C. O. Maher, J. A. Heth, O. Sagher, D. A. Wilkinson, M. Snuderl, S. Venneti, S. H. Ramkissoon, K. A. McFadden, A. Fisher-Hubbard, A. P. Lieberman, T. D. Johnson, X. S. Xie, J. K. Trautman, C. W. Freudiger, and S. Camelo-Piragua, Nat. Biomed. Eng. **1**, 0027 (2017).
7. B. Sarri, R. Canonge, X. Audier, E. Simon, J. Wojak, F. Caillol, C. Cador, D. Marguet, F. Poizat, M. Giovannini, and H. Rigneault, Sci. Reports **9** (2019).
8. C. W. Freudiger, W. Yang, G. R. Holtom, N. Peyghambarian, X. S. Xie, and K. Q. Kieu, Nat. Photonics **8**, 153 (2014).
9. K. Nose, Y. Ozeki, T. Kishi, K. Sumimura, N. Nishizawa, K. Fukui, Y. Kanematsu, and K. Itoh, Opt. Express **20**, 13958 (2012).
10. S. Heuke, B. Sarri, X. Audier, and H. Rigneault, Opt. Lett. **43**, 3582 (2018).
11. G. Dai, K. Katoh, and Y. Ozeki, Opt. Express **29**, 11702 (2021).
12. S. Heuke, B. Sarri, A. Lombardini, X. Audier, and H. Rigneault, Opt. Lett. **43**, 4763 (2018).
13. Y. Ozeki, Y. Kitagawa, K. Sumimura, N. Nishizawa, W. Umemura, S. Kajiyama, K. Fukui, and K. Itoh, Opt. Express **18**, 13708 (2010).
14. X. Audier, S. Heuke, P. Volz, I. Rimke, and H. Rigneault, APL Photonics **5**, 011101 (2020).
15. C. Gohle, J. Rauschenberger, T. Fuji, T. Udem, A. Apolonski, F. Krausz, and T. W. Hänsch, Opt. Lett. **30**, 2487 (2005).
16. S. Brustlein, P. Ferrand, N. Walther, S. Brasselet, C. Billaudeau, D. Marguet, and H. Rigneault, J. Biomed. Opt. **16**, 021106 (2011).